Surface Science 605 (2011) 257–266

Contents lists available at ScienceDirect

Surface Science

journal homepage: www.elsevier.com/ locate/susc

Surface Science Prospectives

Electron beam deposition for nanofabrication: Insights from surface science

J.D. Wnuk [a,b], S.G. Rosenberg [a], J.M. Gorham [a], W.F. van Dorp [c,d], C.W. Hagen [d], D.H. Fairbrother [a,*]

[a] Department of Chemistry, Johns Hopkins University, Baltimore, MD USA 21218
[b] Department of Chemistry, Princeton University, Princeton, New Jersey, USA 08544
[c] Department of Applied Physics, University of Groningen, Groningen, The Netherlands
[d] Delft University of Technology, Faculty of Applied Sciences, Delft, The Netherlands

ARTICLE INFO

Article history:
Received 29 July 2010
Accepted 21 October 2010
Available online 28 October 2010

Keywords:
Electron beam induced deposition
Organometallics
Electron–molecule interactions
Electron–solid interactions
Photoelectron spectroscopy
Mass spectrometry
Electron microscopy

ABSTRACT

Electron beam induced deposition (EBID) is a direct-write lithographic technique that utilizes the dissociation of volatile precursors by a focused electron beam in a low vacuum environment to create nanostructures. Notable advantages of EBID over competing lithographic techniques are that it is a single step process that allows three-dimensional free-standing structures to be created, including features with single-nanometer scale dimensions. However, despite the inherent advantages of EBID, scientific and technological issues are impeding its development as an industrial nanofabrication tool. Perhaps the greatest single limitation of EBID is that metal-containing nanostructures deposited from organometallic precursors typically possess unacceptable levels of organic contamination which adversely affects the material's properties. In addition to the issue of purity, there is also a lack of understanding and quantitative information on the fundamental surface reactions and reaction cross-sections that are responsible for EBID. In this prospective, we describe how surface analytical techniques have begun to provide mechanistic and kinetic insights into the molecular level processes associated with EBID. This has been achieved by observing the effect of electron irradiation on nanometer thick films of organometallic precursors adsorbed onto solid substrates at low temperatures (<200 K) under ultra-high vacuum conditions. Experimental observations include probing changes in surface composition, metal oxidation state, and the evolution of volatile species. Insights into surface reactions associated with purification strategies are also detailed. We also discuss unresolved scientific challenges and opportunities for future EBID research.

1. Introduction

Focused electron beam induced processing (FEBIP) is an emerging lithographic strategy that uses the electron stimulated decomposition of transiently adsorbed, molecular precursors under low vacuum conditions for the purpose of fabricating three-dimensional structures, including features with single-nanometer scale dimensions. FEBIP can induce either surface etching or deposition depending upon the products formed during the electron beam's interaction with the precursor [1]. When the decomposition products react with the substrate to form volatile species, material is removed from the surface in a process referred to as electron beam induced etching. Conversely, deposition occurs when electron stimulated decomposition produces non-volatile fragments in a process called electron beam induced deposition (EBID). The EBID process is the focus of this prospective.

EBID was first identified in the 1930's as the cause of unintentional carbonaceous thin film growth that occurs when surfaces are exposed to electron irradiation under low vacuum conditions [2]. However, in the past few years EBID has attracted interest as a tool for nanofabrication, evidenced by the appearance of several recent review articles [1,3,4]. This interest in EBID can be attributed to the advantages it offers when compared to other nanofabrication technologies, including the ability to create smaller-scaled features in a single-step, direct-write process without the use of resist layers. Depending on the spatial registry of the focused electron beam with respect to the substrate, EBID fabricated nanostructures can be grown vertically and/or horizontally. Currently, EBID is used commercially to repair masks that are used in UV and EUV lithography [5]. EBID is preferable to the traditional repair technique of focused ion beam induced deposition (FIB) because there is no gallium contamination of the mask when a focused electron beam is used [6–8]. EBID is also used commercially to customize tips for scanning probe microscopy (Fig. 1(a)) [9,10].

A particularly important category of EBID materials are the metallic nanostructures deposited by the electron stimulated decomposition of organometallic precursors. A few examples of these types of EBID structures are shown in Fig. 1: cobalt-containing arches straddling two electrodes deposited from cobalt carbonyl, Co_2CO_8 (Fig. 1(b)) [11], an electron emitter device deposited from the

* Corresponding author.
E-mail address: howardf@jhu.edu (D.H. Fairbrother).

0039-6028/$ – see front matter © 2010 Elsevier B.V. All rights reserved.
doi:10.1016/j.susc.2010.10.035

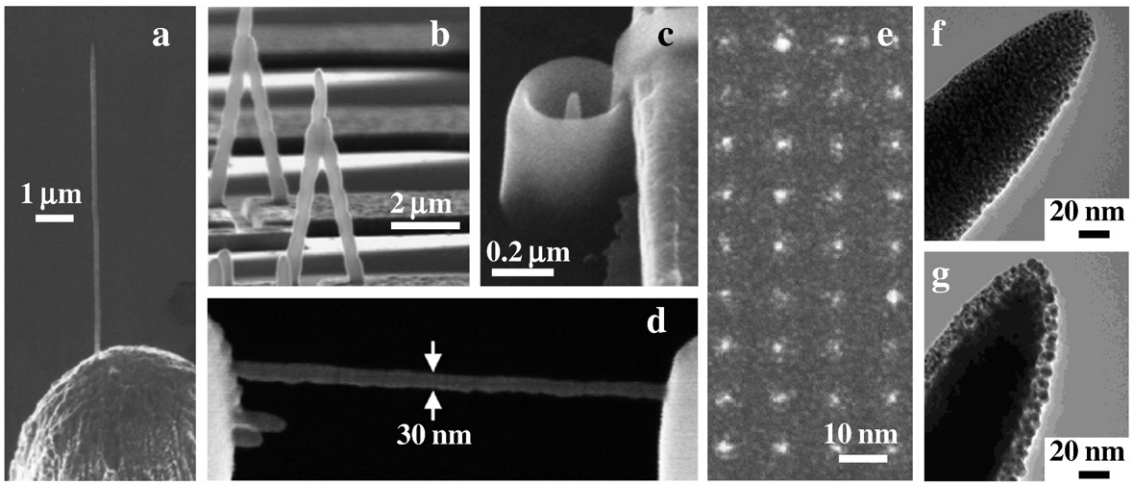

Fig. 1. The electron beam induced decomposition of volatile precursors in a low pressure environment is capable of fabricating a wide variety of free standing nanostructures. (a) Current applications of this technique include modification of scanning probe tips (refs 9 and 10). Metal containing structures are readily deposited from organometallic precursors; for example, structures composed of (b) cobalt (ref 11), (c) platinum on silicon dioxide (ref 12), and (d) platinum (ref 13). (e) A one-step, direct-write process, the deposition resolution of EBID is on the order of single nanometers as shown by an array of nanodots deposited from tungsten hexacarbonyl within a (S)TEM (ref 19). Compositional control of EBID deposits has provided the impetus to develop purification strategies, such as depositing gold (f) directly from $Au^{III}(acac)Me_2$ compared to (g) in the presence of water (ref 24).

sequential electron induced decomposition of tetraethoxysilane, TEOS, and trimethyl-(methylcyclopentadienyl) platinum(IV), $MeCpPt^{IV}Me_3$ (Fig. 1(c)) [12], and a freestanding, platinum containing wire grown horizontally from the $MeCpPt^{IV}Me_3$ precursor (Fig. 1(d)) [13]. EBID can also make or modify nanophotonic and nanoplasmonic devices [14–16]. Another technological push involves using EBID as a tool to fabricate metallic nanostructures with dimensions on the sub-5 nanometer scale, similar to the array shown in Fig. 1(e) [17–19].

Due to the difficulties in controlling chemical composition within metallic EBID nanostructures, substantial efforts have been taken to increase the metal content in deposits by various means of purification [20]. Although post-deposition annealing has been attempted both in-situ [21] and ex-situ [22], these strategies have shown limited potential for removing organic contamination and often result in physical deformation of the nanostructure [13,22,23]; a consequence which nullifies the spatial resolution of the EBID method [13]. Another approach has been to introduce auxiliary reactive species (e.g. water, oxygen) either during deposition, as shown in Fig. 1(f) and (g) [24–26], or during post-deposition annealing [23,27]. However, this approach presently suffers from a lack of reproducibility and still often results in a level of organic contamination which adversely affects the structure's intended material's properties [27–29].

When EBID structures are deposited within an electron microscope they can be imaged using scanning electron microscopy (SEM) or scanning transmission electron microscopy (S)TEM [11,30,31] and/or assayed in terms of their chemical composition, for example by using energy dispersive X-ray spectroscopy (EDX) or Auger electron spectroscopy (AES) [11,32–37]. This information is also often complemented by ex-situ measurements (e.g. conductivity) [11,27,28,38,39]. As a result, characterization of deposited materials has provided a wealth of information on the effect that experimental parameters, such as electron [29,32,40–43] and precursor [44] dose as well as dwell time [31,34,45], have on the deposition rate [46], spatial resolution [16,47], and physical dimensions of EBID structures [17,28]. However, this information does not provide any molecular level insight into how precursors undergo electron-stimulated decomposition or quantitative information on reaction cross-sections. Thus, although typical EBID studies (using apparatus similar to the one shown in Fig. 2(a)), have determined that the electron irradiation of organometallic precursors results in structures containing clusters of metal atoms encased in an amorphous, organic matrix [13,24,48–63], mechanistic insights into how to control the chemical composition and structure of these deposits have yet to be elucidated.

From these observations it is clear that if EBID is to evolve from a set of empirical recipes for producing nanostructures to a viable

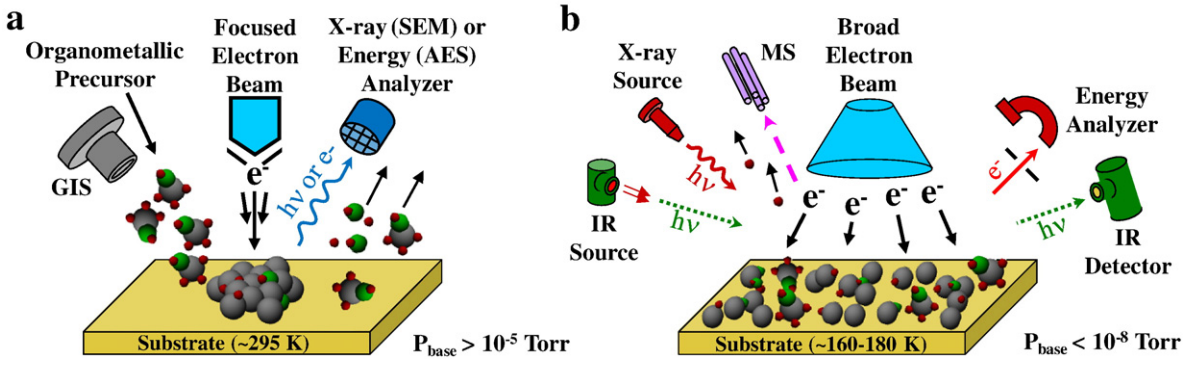

Fig. 2. (a) Focused electron beam induced processing is typically performed using a high energy (5–200 keV), focused electron beam incident upon a surface at room temperature in the presence of transiently adsorbed precursor molecules (<1 ML) introduced as a directed flow from a gas injection system (GIS). (b) Molecular level information on the electron stimulated deposition process can be obtained by irradiating an adsorbed molecular film (1–2 ML) with a broad electron beam (>1 cm^2) over a surface area large enough to facilitate *in-situ* surface and gas phase analysis.

scientific tool for nanofabrication, a better understanding of the interactions between the substrate, electrons, and adsorbed precursor molecules must be developed. This information will help us not only to understand the EBID process at a more detailed level but can also provide a framework that can be used to predict how the deposition conditions influence the composition and properties of the deposit. Amongst the various facets of EBID, the fundamental interactions of electrons with solids are certainly the best understood [64]. For example, a Monte Carlo simulation has recently been constructed that can qualitatively model the electron-substrate interactions involved in EBID [65]. In contrast, electron interactions with adsorbed precursor molecules are significantly less well understood, although a number of dissociation mechanisms have been identified including impact ionization, dissociative electron attachment and electron excitation [66]. The nature and origin of the electrons responsible for dissociation is complicated by the interaction of the incident/primary electron beam with the surface which generates a plume of inelastically backscattered and secondary electrons that may also react with adsorbed species. Even less information is available on the electron stimulated bond breaking events that accompany the decomposition of EBID precursors, even for the gas phase analogs [67,68]. Indeed, this emphasizes the need for more detailed molecular level information on the various elementary surface processes (e.g. diffusion, decomposition) that involve the precursor molecules.

In this prospective, we highlight the capabilities of ultra-high vacuum (UHV) surface analytical techniques to provide mechanistic insights and quantitative data relevant to the EBID process. The experimental approach relies on studying the effect of electron irradiation on adsorbed precursor molecules *in-situ* and in real time. Insights from these studies will provide design criteria for the development of new organometallic precursors that yield EBID materials with greater compositional control. Furthermore, common surface analytical techniques can also provide quantitative information on parameters such as the sticking probabilities of the precursor molecules [69] and the reaction cross-sections for electron stimulated decomposition [70], information which is difficult to obtain from traditional EBID experiments.

2. Experimental methodology

The established EBID approach to create nanostructures is shown schematically in Fig. 2(a). Deposition is performed in an electron microscope system with a focused, high energy electron beam (energies typically between 5 and 200 keV) in a low vacuum (10^{-5} to 10^{-3} Torr) environment. The gas handling systems are typically modified to allow volatile organometallic species to be introduced in a directed flow toward the substrate, using a gas injection system (GIS) [71]. Under ambient temperature conditions, deposits grow when transiently adsorbed precursor molecules decompose at the point of intersection between the incident electron beam and the substrate. Manipulation of the electron beam's spatial registry with respect to the substrate enables two- and three-dimensional nanostructures to be created, such as those shown in Fig. 1.

To develop a molecular level understanding of the deposition process, the effect of electron irradiation on adsorbed precursors must be probed *in-situ* and in real-time. This can be achieved by applying surface, analytical techniques, as shown in Fig. 2(b) [70,72–75].

Indeed, UHV surface science studies have been used successfully to probe electron mediated processes relevant to atmospheric chemistry [66,76–78], astrochemistry [66,79,80], astrobiology [66,81], thin film modification [66,82–86], and radiation damage to biologically relevant molecules [66,84,87,88]. In contrast, relatively few UHV studies have focused on the interactions of electrons with organometallics. Yates et al. have studied the effect of low-energy (2–27 eV) electrons on the decomposition of hexafluoracetylacetonate Cu(I) vinyltrimethylsilane, a metal-organic chemical vapor deposition (MOCVD) precursor used for the deposition of copper [89]. X-ray photoelectron spectroscopy (XPS) results showed that electron stimulated reactions led to the formation of Cu(0) while the threshold for decomposition was ≈4 eV, consistent with a dissociative electron attachment mechanism. However, most studies designed to probe electron-induced reactions of organometallics adsorbed onto solid substrates under UHV conditions have focused on only metal carbonyl precursors (e.g. $Ni(CO)_4$, $Fe(CO)_5$ and $W(CO)_6$) [90–94]. For example, Swanson et al. observed CO desorption during the electron irradiation of $W(CO)_6$ adsorbed onto silicon at 145 K and the formation of partially decarbonylated fragments ($W(CO)_x$, $x<6$) [94]. Using a combination of temperature programmed desorption (TPD) and AES, Henderson et al. have demonstrated that low-energy (3–132 eV) electron decomposition of $Fe(CO)_5$ adsorbed onto Ag[111] converts the parent species into $Fe_x(CO)_y$ clusters, which are much less reactive towards further electron induced chemistry compared to the parent compound [91,92]. By measuring the loss of adsorbed $Fe(CO)_5$ as a function of electron exposure using TPD, the authors were able to determine that the total reaction cross-section for electron stimulated decomposition of adsorbed $Fe(CO)_5$ systematically changed as a function of incident electron energy and was, on average, the same order of magnitude as the value for the gas phase species [91]. The fact that the measured cross-sections are comparable for the gas phase and surface bound species suggests that, for this precursor and electron energy, molecular decomposition is initiated by the incident/primary electron, and furthermore, that surface mediated relaxation processes for any reactive intermediates involved in the decomposition process are insignificant by comparison. A similar experimental approach has also shown that decomposition of benzene-chromium-tricarbonyl by 220 eV electrons is initiated by the cleavage of both Cr–CO and Cr–benzene bonds, with an overall cross-section of $\approx 3\times10^{-17}$ cm^{-2} [95].

The contrast between the operating conditions and information that can be obtained from a typical EBID experiment and an UHV surface science study are compared in Fig. 2(a) and (b) and detailed in Table 1. Although they both involve the electron stimulated decomposition of precursor molecules, analysis of Table 1 reveals that there are a number of important differences and relationships that exist between the deposition conditions that pervade typical EBID experiments (Fig. 2(a)) and those that characterize the UHV studies (Fig. 2(b)); these are the focus of this prospective. For example, in typical EBID experiments, deposition can occur under either precursor limited or current limited conditions [1,4], depending on the relative flux of incident electrons and precursor molecules. In

Table 1
Comparison of two approaches to study electron beam induced deposition; the typical experimental approach used for device fabrication and a surface science strategy for investigating the deposition process.

Experimental parameter	Typical EBID experiment	Surface science approach
Pressure regime (Torr)	10^{-5} to 10^{-3}	$<10^{-8}$
Incident electron energy (keV)	3–200	.04–5
Power density (mW/mm^2)	$\approx 10^2$	$\approx 10^{-2}$
Substrate temperature (K)	≈300	<180
Precursor surface coverage (ML)	<1	1–5
Size scale of deposits	$\approx nm^3$	Nanometer thick; cm^2 2-dimensional footprint
Analytical techniques	SEM, (S)TEM, EDX, AES	XPS, RAIRS, HREELS, MS, TPD
Type of information that can be obtained	Composition, structure and dimensions of EBID materials	Insights into precursor decomposition and kinetics

contrast, the UHV surface science studies occur exclusively within the precursor limited regime due to the fact that there is no incident flux of precursor molecules during irradiation and that all of the molecules are trapped on the surface and undergo complete electron stimulated decomposition. The low substrate temperatures and power densities, coupled with the lack of a partial pressure of precursor molecules, also mean that local heating and diffusion effects which can be important in typical EBID experiments do not influence results obtained in the UHV surface science studies (see Table 1). As a consequence, the UHV surface science studies provide information that applies exclusively to the electron stimulated decomposition of the precursor molecules in the absence of phenomena such as diffusion, incomplete precursor decomposition and possible multi-electron effects (which may become operative at the higher current densities used in typical EBID experiments). The higher coverage of precursor molecules required for the UHV studies also means that any bimolecular processes involving reaction products occur with a greater probability than in typical EBID experiments, where deposition proceeds in the presence of sub-monolayer coverage of precursor molecules (Table 1). One example would be the potential for bimolecular coupling of methyl radicals, formed as a result of metal-methyl bond cleavage during electron irradiation, to form ethane. However, these higher order processes can often be identified in the UHV surface science studies by studying relative product yields as a function of the initial precursor coverage. A notable advantage of the UHV approach is that the chemical composition of EBID structures (with the exception of hydrogen) can be accurately determined without the confounding effects of carbon and oxygen incorporation from the vacuum contaminant gases (notably hydrocarbons and water vapor) which are present at significant partial pressures in typical EBID experiments performed in electron microscopes.

Another important distinction between typical EBID experiments and the UHV surface science approach is that to obtain sufficient signal, surface analytical techniques require an analysis area ($\approx 1\ cm^2$) which is significantly larger than the nanometer-sized features deposited in typical EBID experiments. This requires the experimental paradigm to shift from that of three-dimensional nanostructures to nanometer-scale thin films. These films can be prepared by adsorbing a known thickness of precursor molecules onto a cooled substrate under UHV conditions. To ensure a uniform electron flux within the adsorbate layer, the film's thickness should ideally be in the sub-monolayer regime and certainly at least less than or equal to the inelastic mean free path of the incident electrons. The use of ultra-thin adsorbate films also minimizes the risk of unwanted charging effects during electron irradiation. To ensure that any lower weight molecular species produced during electron irradiation escape into the gas phase where they can be probed by mass spectrometry, an appropriate substrate temperature must be selected that is sufficiently low (<200 K) to adsorb the parent organometallic precursor but not so low as to trap any volatile products (e.g. low molecular weight hydrocarbons). The low temperature UHV approach also benefits from the fact that the non-adiabatic processes involved in EBID, such as electron stimulated decomposition, are temperature independent.

The requirement for comparatively large analysis areas means that the high energy, focused electron beams used in FEBIP must be replaced by a suitably broad beam electron source, such as a diffusive "flood" electron gun that is widely used for applications such as charge neutralization in electron spectroscopy. Consequently, the incident electron energies and power densities in UHV surface science studies are lower than those used in traditional EBID experiments. However, the only major change that occurs when the primary beam energy increases above a few keV is that the yield of secondary electrons continues to change [96]. Furthermore, the low energy secondary electrons (<500 eV) generated by the interaction of a high energy (>5 keV) primary beam with a substrate are believed to make a significant contribution to the EBID process [64]. Another experimental requirement for quantitative kinetic analysis from UHV surface science studies is that the intensity of the incident electron beam is uniform across the surface to ensure that all precursor molecules are exposed to the same electron dose. The spatial distribution of the incident electron flux is best determined with a Faraday cup. [97]

A few of the surface analytical techniques that can probe different aspects of the EBID process are illustrated in Fig. 2(b); changes in the metal center's oxidation state as well as changes in the film's stoichiometry can be monitored using XPS [72,73], while changes in chemical bonding within the adlayer can be monitored with vibrational spectroscopic techniques such as reflection absorption infrared spectroscopy (RAIRS) [72,73] or high resolution electron energy loss spectroscopy (HREELS) [98]. Data from these various techniques can be obtained as a function of electron dose and incident electron energy. In addition, the UHV conditions permit the gas phase products of the decomposition process to be identified using mass spectrometry (MS) [72,73]; information which cannot be obtained in typical EBID experiments due to the presence of a large partial pressure of precursor molecules in the background.

However, not all traditional UHV surface analytical techniques can be used to probe the decomposition process. For example, the high electron fluxes required during AES make it unsuitable as a non-invasive technique for monitoring the electron stimulated decomposition process as a function of irradiation time, although conversely AES can create EBID structures in a fashion analogous to the one shown in Fig. 2(a) [35,53,72,99].

3. Mechanistic insights into EBID

3.1. The deposition process

In this section, we provide examples of mechanistic insights into the electron beam induced decomposition of several EBID precursors acquired using a UHV surface science approach. In addition to the information obtained from individual techniques, these studies highlight the inherent advantages of a combinatorial approach. For example, while XPS and vibrational spectroscopy can probe changes that occur to the condensed phase, mass spectrometry provides complementary information by identifying volatile species ejected into the gas phase.

XPS is perhaps the most useful surface analytical technique due to its ability to measure changes in film composition, thickness, as well as the bonding state of adsorbed species, all as a function of electron dose and/or incident energy. Thus, in Fig. 3(a), changes in the Au(4f) region of adsorbed dimethyl-(acetylacetonate) gold(III) (Au^{III}(acac) Me_2) molecules [72], measured as a function of increasing electron dose, indicate that reduction of the Au(III) atoms associated with the precursor produces a new species with a formal oxidation state consistent with metallic gold, Au(0). Fig. 3(a) also shows that for all electron exposures, the Au(4f) spectra can be deconvoluted by a linear combination of the spectral envelopes from the Au(III) precursor and the metallic product, supporting the idea that no stable intermediates are involved in the decomposition process. In EBID studies, XPS spectral analysis is often facilitated by the comparatively large changes in formal oxidation states of the metal atoms (e.g. Au(III) to Au(0) [72], Pt(IV) to Pt(0) [73]). Analysis of XPS data also reveals that the area of the Au(4f) region remains unchanged (<5% variance) indicating that irradiation does not lead to the electron stimulated desorption of any gold containing species. In principle, photoelectrons generated by the interaction of the primary X-ray beam with the substrate can themselves induce unwanted reactions in organometallic precursors during XPS analysis, including reduction of the central metal atoms [72]. However, the rates of X-ray induced reactions are easily measured independently and to date these effects

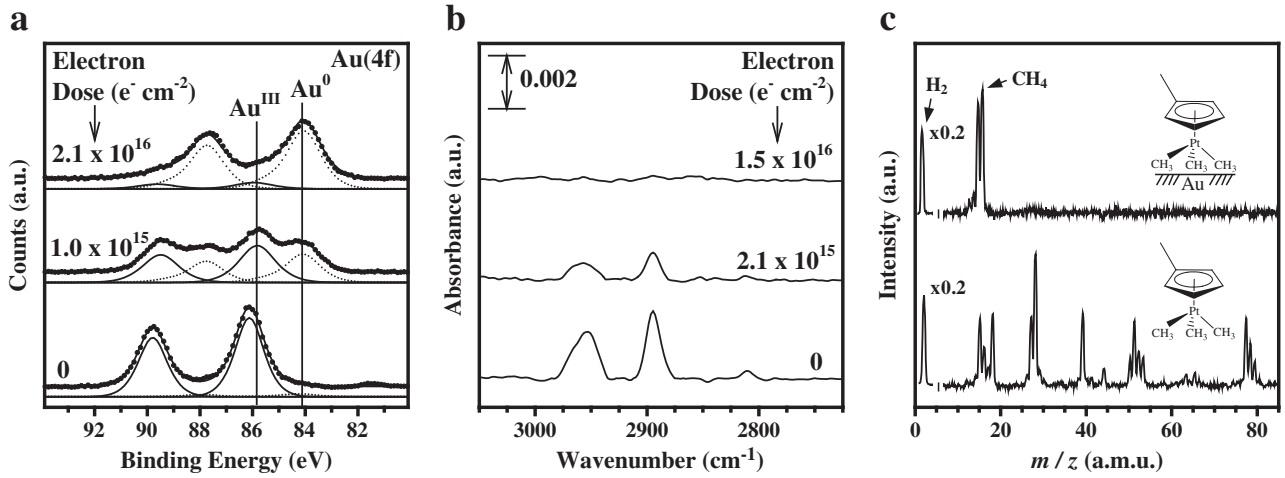

Fig. 3. *In-situ* investigation of the electron stimulated decomposition process enables mechanistic information to be deduced. (a) XPS of $Au^{III}(acac)Me_2$ adsorbed onto a graphite substrate provides information into the effect of increasing electron dose on the metal center's oxidation state. (b) RAIRS illustrates the changes in vibrational intensity in the C–H bonding region during electron irradiation of molecular $MeCpPt^{IV}Me_3$ adsorbed onto gold. (c) A comparison of the MS fragmentation pattern produced from $MeCpPt^{IV}Me_3$ in the gas phase (bottom) and when exposed to electron irradiation while adsorbed onto an inert gold substrate (top).

have not proceeded at a rate that has precluded the use of XPS in following electron stimulated decomposition processes.

Complementary information on the decomposition process can also be obtained from vibrational spectroscopy, as shown in Fig. 3(b), for the C–H stretching region of adsorbed trimethyl-(methylcyclopentadienyl) platinum(IV), $MeCpPt^{IV}Me_3$, molecules [73]. The onset of electron irradiation is observed to produce a systematic decrease in the intensity of vibrational modes associated with the parent molecule in the absence of new spectral features, consistent with the idea that decomposition of adsorbed $MeCpPt^{IV}Me_3$ proceeds without the formation of any stable intermediates. Furthermore, the complete loss of spectral intensity in the C-H region (Fig. 3(b)) occurs over a comparable timescale to the electron induced reduction of Pt (IV) atoms. This indicates that the reduced platinum atoms are formed within a dehydrogenated, amorphous carbonaceous film, whose formation proceeds concomitantly with the electron induced reduction of Pt(IV) atoms, the later measured by XPS [73]. The two most applicable vibrational techniques to study EBID under UHV conditions are RAIRS and HREELS. In many respects, these two techniques have complementary strengths and weaknesses [100]. Due to its superior resolution compared to HREELS, RAIRS is better suited to identifying changes within the ligand architecture that can accompany electron irradiation of organometallic precursors. However, HREELS is better suited to examining changes in metal-ligand bonding due to its ability to examine vibrational modes below $\approx 600\ cm^{-1}$.

Fig. 3(c) highlights the significant influence that phase exerts on the volatile species produced when organometallic EBID precursors are exposed to low energy (<200 eV) electrons [73]. In the gas phase (Fig. 3(c), lower spectra), electron induced decomposition of $MeCpPt^{IV}Me_3$ leads to the production of a wide variety of products, including those associated with the cyclopentadienyl ring and the methyl ligands. In contrast, when the same molecule, adsorbed onto a solid substrate at 180 K, is irradiated with similarly energetic incident electrons, the only volatile carbon-containing product observed is methane (Fig. 3(c), upper spectra).

Additional molecular level insights into the EBID process can be obtained by considering collectively both XPS and MS data on the effects that electron irradiation exert on adsorbed $MeCpPt^{IV}Me_3$ molecules. Thus, XPS measurements revealed that as a consequence of electron induced decomposition, the C:Pt ratio changed from 9:1 to 8:1; independent of the film's thickness [73]. Taken in conjunction with the MS data shown in Fig. 3(c), this result implies that one of the three Pt-CH_3 bonds breaks during the EBID process and leads to methane formation, while the remaining eight carbon atoms associated with the precursor become entrapped and form a carbonaceous film. In principle, these results are also consistent with the idea that cleavage of the C–CH_3 bond associated with the cyclopentadienyl ring is responsible for methane formation and the accompanying change in the film's stoichiometry. However, experiments performed with $CpPt^{IV}Me_3$, which lacks a C–CH_3 bond, revealed that methane was also produced during electron irradiation, supporting the idea that Pt-CH_3 and not C–CH_3 bond cleavage is responsible for the loss of carbon atoms during electron induced decomposition [73].

Recent XPS results obtained with the $Pt(PF_3)_4$ precursor [101] suggest that for this EBID precursor the initial electron mediated process involves ejection of a single PF_3 group, analogous to the single Pt–CH_3 bond breaking process that accompanies electron irradiation of adsorbed $MeCpPt^{IV}Me_3$ [73]. For both precursors, these dissociation events are responsible for well-defined changes in the film's stoichiometry. In contrast, no such well-defined changes in stoichiometry have been observed when two multi-dentate precursors, $Au^{III}(acac)Me_2$ [72] and $Cu^{II}(hfac)_2$, were irradiated. These experimental observations suggest that for precursors that contain multi-dentate ligands, the initial electron stimulated single bond breaking event does not lead to the evolution of discrete molecular species (e.g. PF_3 and CH_3), presumably because the multidentate ligands still remain tethered to the central metal atom following a single metal–ligand bond cleavage event. Thus, our results support the idea that at least under the conditions prevalent in UHV surface science studies (see Table 1), electron stimulated decomposition of EBID precursors is initiated by cleavage of a single metal–ligand bond. However, one potential scenario that warrants further investigation is that under the higher incident electron fluxes that characterize traditional EBID experiments (see Table 1), multiple bond breaking (e.g. the loss of two CH_3 or PF_3 groups from $MeCpPt^{IV}Me_3$ and $Pt(PF_3)_4$, respectively) are possible. Such a process could aid in rationalizing the empirical observation that the carbon content of an EBID deposit often decreases at higher current densities [27].

It is important to note that in EBID, although the initial bond cleavage event must be initiated by an electron stimulated process, subsequent decomposition of the resultant surface bound species can occur by either electron or thermally stimulated processes. Thus, it is possible that for some precursors, the overall EBID process could be a result of an electron initiated but subsequent thermally assisted

process. Such a multi-faceted process is particularly likely to occur in cases where intermediates, such as $Pt(PF_3)_3$, are formed during the electron irradiation process [101].

In UHV studies designed to probe EBID, the use of lower substrate temperatures (<100 K) during irradiation can enable mass spectrometry to be used in the form of a post irradiation TPD technique to identify reaction products [102]. Indeed, this approach has recently been used to study the electron induced decomposition of hexamethyldisiloxane, an EBID precursor for SiO_2 deposition [103]. After performing electron irradiation at a substrate temperature of 40 K, methane was identified as a product by TPD. The advantage of using the substrate as a cryogenic "trap" in this way is that smaller product concentrations can be detected compared to the situation where mass spectrometry is used to identify volatile fragments produced *in-situ* during irradiation. However, reaction products that remain adsorbed during irradiation can experience electron stimulated desorption or secondary reactions; either may complicate an analysis of the fundamental bond breaking processes involved in the electron induced decomposition of the precursor.

3.2. Influence of ligand architecture on gas phase decomposition products

One of the current limitations of EBID is the unacceptably high levels of organic contaminants (principally carbon) that become incorporated into deposits. This is partially a consequence of the fact that the choice of current EBID precursors is largely restricted to organometallics that were initially developed for either chemical vapor deposition (CVD) or atomic layer deposition (ALD) applications. However, the electron stimulated decomposition of organometallics is markedly different from the thermal decomposition processes that accompany CVD and ALD. [104–110]

One approach to mitigate contamination in EBID is to understand how the structure of the organometallic precursor influences the partitioning of the ligand atoms into volatile and non-volatile species, such as in Eq. (1).

$$\text{Precursor}_{(ads)} + e^- \rightarrow \text{Products}_{(ads)} + \text{Products}_{(g)} \quad (1)$$

Towards this goal, the volatile (neutral) fragments produced from a number of organometallic precursors during electron irradiation have been identified using mass spectrometry, as shown in Fig. 4. Analysis of these products reveals that the chemical identity of the volatile species varies systematically as a function of the precursor's ligand architecture. Thus, adsorbed bis-methylcyclopentadienyl nickel(II) ($Ni^{II}(MeCp)_2$) produces only hydrogen during electron irradiation and does not generate any volatile carbon-containing products. In contrast, the electron stimulated reactions of the two platinum precursors, $MeCpPt^{IV}Me_3$ and $CpPt^{IV}Me_3$, release methane as a result of one $Pt–CH_3$ bond cleavage event, as discussed previously. Collectively, these results suggest that all of the carbon atoms contained in the cyclopentadienyl and methylcyclopentadienyl ligands become trapped within EBID deposits, at least under deposition conditions that characterize the UHV surface science approach described in Table 1.

Consequently, these comparatively large and carbon-rich ligands should be avoided when designing precursors specifically for EBID. Fig. 4 shows that methane is also produced when the gold precursor, $Au^{III}(acac)Me_2$, is irradiated, suggesting that at least some of the carbon atoms in the $Au–CH_3$ bonds will also be released as methane

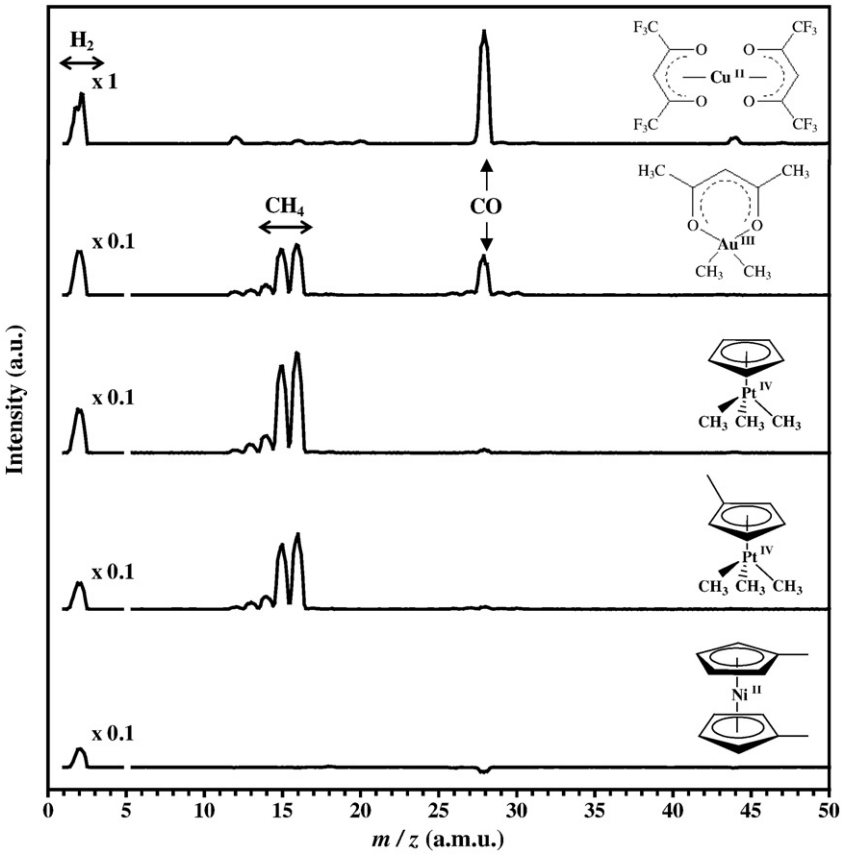

Fig. 4. The mass spectra (0–50 amu) of the volatile neutral species produced when five different organometallic precursors, adsorbed onto a gold substrate at 100 K, were electron irradiated. In each case the thickness of the adsorbed film was 2.0–2.4 nm, the electron beam flux was 1.7×10^{14} electrons/cm^2 s, and the incident electron energy was 500 eV. Each mass spectrum was acquired during the initial (0–20 s) period of irradiation, and background subtracted using the mass spectrum obtained when the clean gold substrate was electron irradiated at the same fluence and incident energy.

during the deposition process. Indeed, collectively the data shown in Fig. 4 for $Ni^{II}(MeCp)_2$, $MeCpPt^{IV}Me_3$, $CpPt^{IV}Me_3$ and $Au^{III}(acac)Me_2$ suggests that a ligand architecture that includes a single M–CH_3 bond may decompose to form a carbon-free deposit. Additionally, a comparison of the uppermost two mass spectra in Fig. 4 indicates that carbon monoxide is liberated from acetylacetonate type ligands during electron irradiation, although XPS analysis of the deposit indicates that a measureable fraction of the oxygen atoms remain. Thus, the release of carbon monoxide would appear to be one of several potential reaction pathways for a multidentate ligand that contains an acetylacetonate ligand. Changes in the adsorbate layer containing the copper precursor, copper(II) hexafluoroacetylacetonate, reveal that fluorine atoms are also being lost as a result of electron irradiation, most likely in the form of gas phase fluoride anions.

It is worth noting that the systematic trends observed in Fig. 4 have all been identified without discussing the metal center, implying that it is the ligand architecture which is principally responsible for the decomposition pathways. If this assertion is verified for a wider range of precursors, then the volatile carbon-containing fragments released during electron irradiation can be predicted based solely on the ligand architecture.

3.3. Purification

In addition to the deposition process, surface analytical techniques can also investigate new purification strategies, for example the removal of organic contaminants from EBID structures using atomic radicals [27,61,75]. The advantage of atomic radicals is that they offer the potential to purify deposits at room temperature by utilizing the intrinsic chemical reactivity of atomic species, specifically atomic hydrogen (AH) and atomic oxygen (AO).

Fig. 5 illustrates how *in-situ* surface analytical methods and *ex-situ* materials characterization techniques have been used to investigate these radical purification strategies [75]. *In-situ* XPS analysis has shown that both AO and AH are capable of removing the vast majority of the contaminant carbon atoms from an EBID thin film deposited from $Au^{III}(acac)Me_2$. However, AO is both more efficient than AH and is capable of removing essentially all of the carbon atoms from a nanometer-scale thick deposit [75]. One of the drawbacks of AO is that it also oxidizes metallic gold atoms at the surface of the EBID deposit to form an oxidized gold species, as evidenced by binding energy shifts in both the O(1 s) and Au(4f) XP spectral regions [75]. However, this oxide can itself be rapidly reduced to metallic gold by exposure to AH. Therefore, a combination of AO followed by AH exposure leads to the formation of a purely metallic gold structure as shown by XPS in Fig. 5(a).

Ex-situ AFM is complementary to UHV surface analysis, providing information on the effect of purification on the physical size of EBID deposits (Fig. 5(b)) [75]. Analysis of the two AFM images in Fig. 5(b) indicates that radical purification decreases the size of EBID deposits. Based on the average chemical composition of the electron beam deposits ($AuC_6O_{0.8}$) determined by XPS and the atomic radii of the constituent elements, the loss of all carbon and oxygen from the film as a result of AO and AH exposure would produce a ≈50% decrease in the volume of material present within the deposits. Assuming that the particles shown in Fig. 5 are spherical, this predicted change in volume is comparable to the 18% decrease in height that was observed

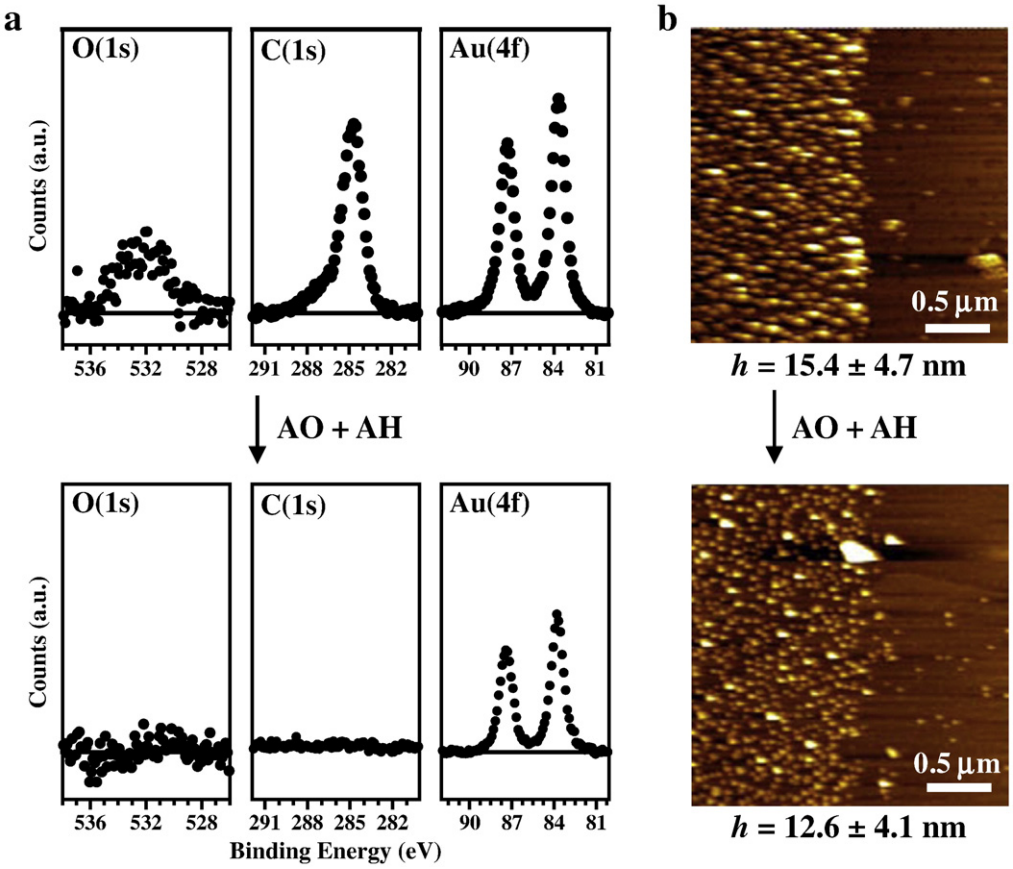

Fig. 5. Atomic radical abatement of organic contamination from EBID deposits. (a) XPS analysis of an amorphous film containing gold, carbon and oxygen (deposited by the electron irradiation of an adsorbed $Au^{III}(acac)Me_2$ layer) before (top) and after (bottom) exposure to a sequence of atomic oxygen (AO) and then atomic hydrogen (AH). (b) *Ex-situ* AFM analysis of particles deposited by rastering an electron beam over a HOPG substrate in the presence of transiently adsorbed $Au^{III}(acac)Me_2$ before (top) and after (bottom) exposure to AO and then AH. *h* is the average height of the particles.

experimentally, from an initial value of 15.4 ± 4.7 nm for the "as deposited" EBID material to 12.6 ± 4.1 nm after exposure to AO and then AH. This observation is also consistent with the idea that radical purification produces consolidated gold particles rather than a honeycomb structure, although verification will require direct observation of the microstructure using SEM or TEM. Although these results indicate that atomic radicals are an effective post deposition purification strategy, their effectiveness as an *in-situ* approach for removing organic contaminants *during* deposition has recently been shown to be compromised by their reactions with unreacted precursor molecules which causes non-area selective deposition [111].

4. Determining total reaction cross-sections

In EBID, the total reaction cross-section, σ_E, represents the probability of an incident electron with energy, E, decomposing an adsorbed precursor molecule. The designation of a *total* reaction cross-section indicates that the value refers to the integrated probability of the primary or secondary electrons initiating decomposition, the latter formed by the interaction of the primary beam with the substrate, through all possible electron initiated intermediates and excitation pathways [66,112]. In typical EBID experiments (illustrated in Fig. 2(a)), σ_E has been approximated by evaluating the increase in volume of deposited material that occurs with increasing electron irradiation [46]. However, in the UHV surface science approach, σ_E can be quantitatively determined directly through Eq. (2), using the fact that in the precursor limited decomposition regime EBID almost always exhibits first-order kinetics with respect to electron dose,

$$\sigma_E = \frac{-\ln\left(C/C_0\right)}{D}, \tag{2}$$

where C/C_0 is the fraction of parent precursor molecules that have decomposed after an electron dose, D. The electron dose can be calculated using Eq. (3),

$$D = \frac{I*t}{A}, \tag{3}$$

where I is the target current (electrons s^{-1}), t is the irradiation time (s), and A is the area of the substrate (cm^2). To most accurately determine D: (a) a Faraday cup should be used, and (b) the flux of incident electrons must be uniformly distributed over the substrate.

A number of surface analytical techniques can be used to determine σ_E, each of which relies on measuring changes in the adlayer as a function of electron dose and/or energy. Each approach has advantages and disadvantages.

4.1. Temperature programmed desorption (TPD)

Measures the change in precursor concentration after a single electron dose using thermal desorption, as shown in Fig. 6(a) [73,91,93,95]. This technique is easy to implement, requiring only the ability to increase the substrate temperature and the presence of a mass spectrometer in close proximity to the sample. Limiting factors are that it is a destructive technique and thus time consuming. Furthermore, if thermal decomposition of the precursor occurs during annealing this will complicate a determination of σ_E.

4.2. Mass spectrometry (MS)

MS can monitor the production rate of volatile species during electron irradiation. This technique provides rapid real-time analysis, providing a full kinetic profile from each adsorbate layer. However, for some species (e.g. H_2) the signal from residual gases in the vacuum chamber must be subtracted from the measured data.

4.3. X-ray photoelectron spectroscopy

XPS monitors changes in the metal center's oxidation state, thereby providing a direct measure of electron induced reduction (see Fig. 3(a)). Multiple data points can be obtained from a single film as a function of electron dose. However, the X-ray sensitivity of each precursor must be checked and if observed makes the experiment more time consuming [72]. XPS analysis also requires accurate spectral deconvolution.

4.4. Reflection absorption infrared spectroscopy (RAIRS)

A non-destructive technique, RAIRS can measure the total reaction cross-section by measuring changes in the intensity of the precursor molecule's vibrational modes as a function of electron dose. However, thicker films are required due to the relatively poor sensitivity of RAIRS and baseline subtraction may complicate quantitative analysis

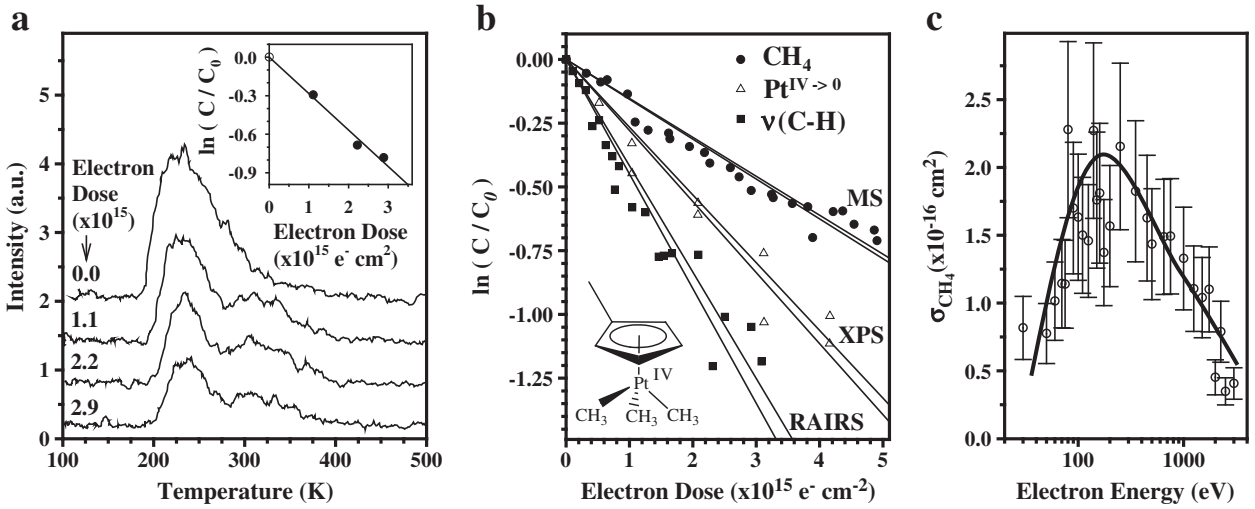

Fig. 6. By monitoring the rate of various surface and gas phase processes, the total reaction cross-section, σ_E, can be determined. For $MeCpPt^{IV}Me_3$, (a) temperature programmed desorption can calculate σ_E by measuring the rate of loss of parent molecules as a result of electron irradiation, (b) XPS, IR and MS data, measured as a function of the electron dose, can also be used to determine σ_E, (c) The reaction cross-section for methane production from $MeCpPt^{IV}Me_3$, measured as a function of the incident electron energy.

of peak areas. In general, vibrational techniques such as RAIRS and HREELS are best suited to identifying intermediate species formed during EBID.

The success of these various surface analytical techniques in determining σ_E is illustrated in Fig. 6(a) and (b) for the electron stimulated decomposition of the platinum precursor, $MeCpPt^{IV}Me_3$, by showing that ln $([MeCpPt^{IV}Me_3]_{D=d}/[MeCpPt^{IV}Me_3]_{D=0})$ decreases linearly as a function of electron dose, consistent with the expectations of Eq. (2). Furthermore, the calculated values of σ_E measured from TPD (2.8×10^{-16} cm^2), MS (9.8×10^{-17} cm^2), XPS (1.4×10^{-16} cm^2) and RAIRS (4.3×10^{-16} cm^2) are all similar to one another (within a factor of 4 although the values were measured using different experimental apparatus). It should be noted that this type of kinetic analysis is typically restricted to the initial period ($C/C_0\approx1/e$) of the loss process. The reasons for this are that the presence of decomposition products, whose concentration will increase with electron dose, may influence the reaction cross-section. Furthermore, for some analytical techniques (e.g. XPS), accurate spectral deconvolution becomes increasingly difficult when the fractional coverage of residual precursor molecules has decreased significantly.

In Fig. 6(a) and (b), reaction cross-sections were determined for the same incident electron energy. However, since the incident electron energy often varies between different EBID experiments, it is useful to know how σ_E varies as a function of the incident electron energy. Energy dependent cross-section measurements can be determined using the experimental approach described in Fig. 2(b). These results, performed using $MeCpPt^{IV}Me_3$ and shown in Fig. 6(c), exhibit a maximum in the total reaction cross-section between 150 and 200 eV [70]; a similar σ_E dependence has been observed for the gold precursor, $Au^{III}(acac)Me_2$ [72].

5. Future research needs and opportunities

A number of important research issues must be addressed if progress in developing EBID as a tool for nanofabrication is to continue. These include:

(1) UHV studies conducted under conditions more representative of those used in typical EBID experiments (see Table 1), such as utilizing high power density electron sources capable of uniformly irradiating a comparatively large (≈1 cm^2) area. Data from these experiments will enable a determination of how the fundamental surface processes respond to changes in incident electron flux, for example. Another important issue that must be addressed is the effect that vacuum contaminants, specifically water vapor and hydrocarbons present in electron microscopes, have on the composition, microstructure and properties of EBID structures.

(2) Surface science studies to be performed on organometallic molecules that exhibit, (i) the same metal center but systematic differences in ligand architecture, and (ii) the same ligand architecture but different metal centers. As part of this effort, EBID practitioners will need to collaborate with inorganic chemists to design new precursors. This will allow important ligand structure–function relationships to be uncovered that relate the structure of organometallic precursors to the chemical composition and microstructure of EBID materials. This information can also guide the rationale design of new precursors with the goal of improving the purity of EBID nanostructures.

(3) To date, efforts have focused on identifying neutral species produced during electron irradiation of organometallic precursors. Studies are needed that focus on identifying the nature of *charged* (both positive and negative) fragments (e.g. F^-) produced from various ligand architectures during EBID.

(4) More quantitative information on fundamental surface processes. For example, the deposition rate, R, of an EBID deposit is determined by various surface kinetic parameters, including the sticking probability of the precursor molecule, the total reaction cross-section and the residence time of the parent precursor molecules on the surface [113]. The need for more quantitative information on these processing parameters is highlighted by the fact that a sticking probability of unity is often assumed in EBID models, although this value is certainly too high. Sticking probabilities can be quantitatively determined using the modified King and Wells method [69]. In this approach, the decrease in the reflected intensity of a molecular beam (composed of gas phase species of interest such as precursor molecules) is measured due to adsorption, when a surface is inserted into the beam path as compared to an inert substrate. However, the authors are not aware of any such studies using EBID precursors. Molecular diffusion also influences the physical dimensions of deposits formed using EBID and identical values are often assumed for diffusion on clean substrates and the surfaces formed during deposition; an assumption that is likely incorrect [114]. Low temperature scanning tunneling microscopy (STM) experiments of surface bound organometallic precursors have the potential to measure diffusion rates of precursor molecules.

(5) A more detailed theoretical, molecular level understanding of the sequence of bond breaking events that accompany the decomposition of adsorbed precursors, including the nature of the excitation process. To aid in this effort, it would be helpful to have information on the reactions of EBID precursors with electrons in the gas phase, including product identification and reaction cross-sections measured as a function of the incident electron energy. As such, this information can form a valuable starting point to rationalize the electron induced reactions of the same molecules in the adsorbed phase; unfortunately, except for a few isolated cases (e.g. $Pt(PF_3)_4$) [68], information even on electron stimulated reactions with gas phase organometallic species used in EBID is limited.

(6) In principle, the electron stimulated decomposition of an organometallic EBID precursor adsorbed onto a solid substrate can be initiated either by the primary electron or the low energy secondary/backscattered electrons generated by the interaction of the primary electron with the substrate. Consequently, σ_E vs. E measurements can provide insights into the relative importance of primary vs. secondary electrons in EBID. However, results to date have not generated a clear consensus as to which electrons are primarily responsible for the decomposition process. This question also has ramifications for the minimum deposit size and the precision with which a deposit can be located [115]. To determine the relative importance of secondary vs. primary electrons, both the yield and energy distribution of secondary/backscattered electrons must be determined in an experimental design that also allows for the simultaneous determination of the reaction efficiency.

Acknowledgements

The authors would like to acknowledge Theodore Madey for his contributions to this research and for introducing many of us to electron beam induced deposition (EBID). Support was provided by the National Science Foundation (Grant No. CHE-0616873). The authors also acknowledge the use of the surface analysis laboratory at The Johns Hopkins University.

References

[1] I. Utke, P. Hoffman, J. Melngailis, J. Vac. Sci. Technol. B 26 (2008) 1197.
[2] R.L. Stewart, Phys. Rev. 45 (1934) 488.
[3] S.J. Randolph, J.D. Fowlkes, P.D. Rack, Crit. Rev. Solid State Mater. Sci. 31 (2006) 55.

[4] W.F. van Dorp, C.W. Hagen, J. Appl. Phys. 104 (2008) 081301.
[5] A. Perentes, P. Hoffmann, Chem. Vap. Deposition 13 (2007) 176.
[6] K. Edinger, et al., J. Vac. Sci. Technol. B 22 (2004) 2902.
[7] T. Liang, E. Frendberg, B. Lieberman, A. Stivers, J. Vac. Sci. Technol. B 23 (2005) 3101.
[8] C.T.H. Heerkens, M.J. Kamerbeek, W.F. van Dorp, C.W. Hagen, J. Hoekstra, Microelectron. Eng. 86 (2009) 961.
[9] B. Hubner, H.W.P. Koops, H. Pagnia, N. Sotnik, J. Urban, M. Weber, Ultramicroscopy 42–44 (1992) 1519.
[10] I.-C. Chen, L.-H. Chen, C. Orme, A. Quist, R. Lal, S. Jin, Nanotechnology 17 (2006) 4322.
[11] Y.M. Lau, P.C. Chee, J.T.L. Thong, V. Ng, J. Vac. Sci. Technol. A 20 (2002) 1295.
[12] K. Murakami, M. Takai, J. Vac. Sci. Technol. B 22 (2004) 1266.
[13] S. Frabboni, G.C. Gazzadi, A. Spessot, Phys. E 37 (2007) 265.
[14] S. Graells, R. Alcubilla, G. Badenes, R. Quidant, Appl. Phys. Lett. 91 (2007) 121112.
[15] A. Weber-Bargioni, A. Schwartzberg, M. Schmidt, B. Harteneck, D.F. Ogletree, P.J. Schuck, S. Cabrini, Nanotechnology 21 (2010) 065306.
[16] H.W.P. Koops, O.E. Hoinkis, M.E.W. Honsberg, R. Schmidt, R. Blum, G. Bottger, A. Kuligk, C. Liguda, M. Eich, Microelectron. Eng. 57–58 (2001) 995.
[17] M. Tanaka, M. Shimojo, M. Han, K. Mitsuishi, K. Furuya, Surf. Interface Anal. 37 (2005) 261.
[18] L. van Kouwen, A. Botman, C.W. Hagen, Nano Lett. 9 (2009) 2149.
[19] C.W. Hagen, W.F. van Dorp, P.A. Crozier, J. Phys. Conf. Ser. 126 (2008) 012025.
[20] A. Botman, J.J.L. Mulders, C.W. Hagen, Nanotechnology 20 (2009) 372001.
[21] R.M. Langford, T.-X. Wang, D. Ozkaya, Microelectron. Eng. 84 (2007) 784.
[22] M.H. Ervin, D. Chang, B. Nichols, A. Wickenden, J. Barry, Melngailis, J. Vac. Sci. Technol. B 25 (2007) 2250.
[23] A. Botman, J.J.L. Mulders, R. Weemaes, S. Mentink, Nanotechnology 17 (2006) 3779.
[24] K. Molhave, D.N. Madsen, A.M. Rasmussen, A. Carlsson, C.C. Appel, M. Brorson, C.J.H. Jacobsen, P. Boggild, Nano Lett. 3 (2003) 1499.
[25] A. Folch, J. Tejada, C.H. Peters, M.S. Wrighton, Appl. Phys. Lett. 66 (1995) 2080.
[26] R.M. Langford, D. Ozkaya, J. Sheridan, R. Chater, Microsc. Microanal. 10 (2004) 1122.
[27] A. Botman, M. Hesselberth, J.J.L. Mulders, Microelectron. Eng. 85 (2008) 1139.
[28] J. Barry, M.H. Ervin, J. Molstad, A. Wickenden, T. Brintlinger, P. Hoffman, J. Melngailis, J. Vac. Sci. Technol. B 24 (2006) 3165.
[29] F. Porrati, R. Sachser, M. Huth, Nanotechnology 20 (2009) 195301.
[30] I. Sychugov, Y. Nakayama, K. Mitsuishi, J. Phys. Chem. C 113 (2009) 21516.
[31] W.F. van Dorp, C.W. Hagen, P.A. Crozier, P. Kruit, J. Vac. Sci. Technol. B 25 (2007) 2210.
[32] R. Cordoba, J. Sese, J.M. De Teresa, M.R. Ibarra, Microelectron. Eng. 87 (2010) 1550.
[33] L. Bernau, M. Gabureac, I. Utke, Condens. Matter (2010)arXiv:1002.2156v1, Preprint.
[34] K.L. Klein, S.J. Randolph, J.D. Fowlkes, L.F. Allard, H.M. Meyer III, M.L. Simpson, P.D. Rack, Nanotechnology 19 (2008) 345705.
[35] A. Luisier, I. Utke, T. Bret, F. Cicoira, R. Hauert, S.-W. Rhee, P. Doppelt, P. Hoffmann, J. Electrochem. Soc. 151 (2004) C535.
[36] T. Lukasczyk, M. Schirmer, H.-P. Steinruck, H. Marbach, Small 4 (2008) 841.
[37] F. Cicoira, P. Hoffmann, C.O.A. Olsson, N. Xanthopoulos, H.J. Mathieu, P. Doppelt, Appl. Surf. Sci. 242 (2005) 107.
[38] H. Hiroshima, N. Suzuki, N. Ogawa, M. Komuro, Jpn. J. Appl. Phys. 38 (1999) 7135.
[39] I. Utke, P. Hoffman, B. Dwir, K. Leifer, E. Kapon, P. Doppelt, J. Vac. Sci. Technol. B 18 (2000) 3168.
[40] P.D. Rack, J.D. Fowlkes, S.J. Randolph, Nanotechnology 18 (2007) 465602.
[41] V. Friedli, I. Utke, K. Molhave, J. Michler, Nanotechnology 20 (2009) 385304.
[42] M. Toth, C.J. Lobo, G. Hartigan, W.R. Knowles, J. Appl. Phys. 101 (2007) 054309.
[43] T. Bret, I. Utke, A. Bachmann, P. Hoffman, Appl. Phys. Lett. 83 (2003) 4005.
[44] M. Tanaka, M. Shimojo, K. Mitsuishi, K. Furuya, Appl. Phys. A 78 (2004) 543.
[45] J.D. Fowlkes, P.D. Rack, Nano 4 (2010) 1619.
[46] A. Botman, D.A.M. de Winter, J.J.L. Mulders, J. Vac. Sci. Technol. B 26 (2008) 2460.
[47] D.J. Burbridge, S.N. Gordeev, Nanotechnology 20 (2009) 285308.
[48] M. Weber, H.W.P. Koops, M. Rudolph, J. Kretz, G. Schmidt, J. Vac. Sci. Technol. B 13 (1995) 1364.
[49] G. Xie, M. Song, K. Mitsuishi, K. Furuya, Appl. Surf. Sci. 241 (2005) 91.
[50] I. Utke, T. Bret, D. Laub, P.A. Buffat, L. Scandella, P. Hoffman, Microelectron. Eng. 73–74 (2004) 553.
[51] H. Plank, C. Gspan, M. Dienstleder, G. Kothleitner, F. Hofer, Nanotechnology 19 (2008) 485302.
[52] H.W.P. Koops, A. Kaya, M. Weber, J. Vac. Sci. Technol. B 13 (1995) 2400.
[53] F. Cicoira, K. Leifer, P. Hoffman, I. Utke, B. Dwir, D. Laub, P.A. Buffat, E. Kapon, P. Doppelt, J. Cryst. Growth 265 (2004) 619.
[54] K. Murakami, et al., Jpn. J. Appl. Phys. 48 (2009) 06FF12.
[55] M. Takeguchi, M. Shimojo, K. Furuya, Jpn. J. Appl. Phys. 46 (2007) 6183.
[56] I. Utke, A. Luisier, P. Hoffman, D. Laub, P.A. Buffat, Appl. Phys. Lett. 81 (2002) 3245.
[57] G.C. Gazzadi, S. Frabboni, J. Vac. Sci. Technol. B 23 (2005) L1.
[58] M. Weber, M. Rudolph, J. Kretz, H.W.P. Koops, J. Vac. Sci. Technol. B 13 (1995) 461.
[59] I. Utke, B. Dwir, K. Leifer, F. Cicoira, P. Doppelt, P. Hoffman, E. Kapon, Microelectron. Eng. 53 (2000) 261.
[60] A. Perentes, G. Sinicco, G. Boero, B. Dwir, P. Hoffman, J. Vac. Sci. Technol. B 25 (2007) 2228.
[61] K. Murakami, S. Nishihara, N. Matsubara, S. Ichikawa, F. Wakaya, M. Takai, J. Vac. Sci. Technol. B 27 (2009) 721.
[62] S. Frabboni, G.C. Gazzadi, L. Felisari, A. Spessot, Appl. Phys. Lett. 88 (2006) 213116.
[63] K. Murakami, N. Matsubara, S. Ichikawa, F. Wakaya, M. Takai, J. Vac. Sci. Technol. B 28 (2010) C2C13.
[64] J.D. Fowlkes, S.J. Randolph, P.D. Rack, J. Vac. Sci. Technol. B 23 (2005) 2825.
[65] D.A. Smith, J.D. Fowlkes, P.D. Rack, Small 4 (2008) 1382.
[66] C.R. Arumainayagam, H.-L. Lee, R.B. Nelson, D.R. Haines, R.P. Gunawardane, Surf. Sci. Rep. 65 (2010) 1.
[67] B.C. Hale, J.S. Winn, J. Chem. Phys. 81 (1984) 1050.
[68] J.F. Friedman, T.M. Miller, J.K. Friedman-Schaffer, A.A. Viggiano, G.K. Rekha, A.E. Stevens, J. Chem. Phys. 128 (2008) 104303/1.
[69] A. Hopkinson, X.-C. Guo, J.M. Bradley, D.A. King, J. Chem. Phys. 99 (1993) 8262.
[70] W.F. van Dorp, J.D. Wnuk, J.M. Gorham, D.H. Fairbrother, T.E. Madey, C.W. Hagen, J. Appl. Phys. 106 (2009) 074903.
[71] V. Friedli, I. Utke, J. Phys. D Appl. Phys. 42 (2009) 125305.
[72] J.D. Wnuk, J.M. Gorham, S.G. Rosenberg, W.F. van Dorp, T.E. Madey, C.W. Hagen, D.H. Fairbrother, J. Appl. Phys. 107 (2010) 054301.
[73] J.D. Wnuk, J.M. Gorham, S.G. Rosenberg, W.F. van Dorp, T.E. Madey, C.W. Hagen, D.H. Fairbrother, J. Phys. Chem. C 113 (2009) 2487.
[74] J.D. Wnuk, J.M. Gorham, D.H. Fairbrother, J. Phys. Chem. C 113 (2009) 12345.
[75] J.D. Wnuk, J.M. Gorham, S.G. Rosenberg, T.E. Madey, C.W. Hagen, D.H. Fairbrother, J. Vac. Sci. Technol. B 28 (2010) 527.
[76] C.C. Perry, G.M. Wolfe, A.J. Wagner, J. Torres, N.S. Faradzhev, T.E. Madey, D.H. Fairbrother, J. Phys. Chem. B 107 (2003) 12740.
[77] A.J. Wagner, C. Vecitis, D.H. Fairbrother, J. Phys. Chem. B 106 (2002) 4432.
[78] N. Nakayama, S.C. Wilson, L.E. Stadelmann, H.-L.D. Lee, C.A. Cable, C.R. Arumainayagam, J. Phys. Chem. B 108 (2004) 7950.
[79] G.A. Kimmel, T.M. Orlando, J. Chem. Phys. 101 (1994) 3282.
[80] G.A. Kimmel, T.M. Orlando, Phys. Rev. Lett. 77 (1996) 3983.
[81] A. Lafosse, M. Bertin, A. Domaracka, D. Pliszka, E. Illenberger, R. Azria, Phys. Chem. Chem. Phys. 8 (2006) 5564.
[82] P. Swiderek, C. Jäggle, D. Bankmann, E. Burean, J. Phys. Chem. C 111 (2007) 303.
[83] P. Swiderek, Eur. Phys. J. D 35 (2005) 355.
[84] S.-P. Breton, M. Michaud, C. Jäggle, P. Swiderek, L. Sanche, J. Chem. Phys. 121 (2004) 11240.
[85] L.D. Weeks, L.L. Zhu, M. Pellon, D.R. Haines, C.R. Arumainayagam, J. Phys. Chem. C 111 (2007) 4815.
[86] T.D. Harris, D.H. Lee, M.Q. Blumberg, C.R. Arumainayagam, J. Phys. Chem. 99 (1995) 9530.
[87] D. Klyachko, T. Gantchev, M.A. Huels, L. Sanche, Spec. Publ. R. Soc. Chem. 204 (1997) 85.
[88] D.V. Klyachko, M.A. Huels, L. Sanche, Radiat. Res. 151 (1999) 177.
[89] S. Mezhenny, I. Lyubinetsky, W.J. Choyke, J.T. Yates, J. Appl. Phys. 85 (1999) 3368.
[90] J.S. Foord, R.B. Jackman, Surf. Sci. 171 (1986) 197.
[91] M.A. Henderson, R.D. Ramsier, J.T. Yates, Surf. Sci. 259 (1991) 173.
[92] M.A. Henderson, R.D. Ramsier, J.T. Yates, J. Vacuum Sci. Technol. Vacuum Surf. Films 9 (1991) 1563.
[93] R.D. Ramsier, M.A. Henderson, J.T. Yates, Surf. Sci. 257 (1991) 9.
[94] J.R. Swanson, F.A. Flitsch, C.M. Friend, Surf. Sci. 215 (1989) L293.
[95] R.D. Ramsier, J.T. Yates, Surf. Sci. 289 (1993) 39.
[96] C.G.H. Walker, M.M. El-Gomati, A.M.D. Assa'd, M. Zadrazil, Scanning 30 (2008) 365.
[97] J.T. Yates Jr., Experimental Innovations in Surface Science: A Guide to Practical Laboratory Methods and Instruments, AIP Press, 1997.
[98] M.N. Hedhili, J.H. Bredehoeft, P. Swiderek, J. Phys. Chem. C 113 (2009) 13282.
[99] S. Wang, Y.-M. Sun, Q. Wang, J.M. White, J. Vac. Sci. Technol. B 22 (2004) 1803.
[100] J.C. Vickerman, I.S. Gilmore, Surface Analysis - The Principal Techniques, 2nd Edition, John Wiley & Sons Ltd, 2009.
[101] K. Landheer, S. Rosenberg, C.W. Hagen, D.H. Fairbrother, manuscript in preparation.
[102] E. Burean, I. Ipolyi, T. Hamann, P. Swiderek, Int. J. Mass Spectrom. 277 (2008) 215.
[103] I. Ipolyi, E. Burean, T. Hamann, M. Cingel, S. Matejcik, P. Swiderek, Int. J. Mass Spectrom. 282 (2009) 133.
[104] B.B. Burton, M.P. Boleslawski, A.T. Desombre, S.M. George, Chem. Mater. 20 (2008) 7031.
[105] M. Dai, J. Kwon, M.D. Halls, R.G. Gordon, Y.J. Chabal, Langmuir 26 (2010) 3911.
[106] J.D. Ferguson, A.R. Yoder, A.W. Weimer, S.M. George, Appl. Surf. Sci. 226 (2004) 393.
[107] M.D. Groner, F.H. Fabreguette, J.W. Elam, S.M. George, Chem. Mater. 16 (2004) 639.
[108] X. Jiang, T.M. Gur, F.B. Prinz, S.F. Bent, Chem. Mater. 22 (2010) 3024.
[109] J. Kwon, M. Dai, M.D. Halls, E. Langereis, Y.J. Chabal, R.G. Gordon, J. Phys. Chem. C 113 (2009) 654.
[110] J.T. Tanskanen, J.R. Bakke, S.F. Bent, T.A. Pakkanen, Langmuir 26 (2010) 11899.
[111] H. Miyazoe, I. Utke, H. Kikuchi, S. Kiriu, V. Friedli, J. Michler, K. Terashima, J. Vac. Sci. Technol. B 28 (2010) 744.
[112] L.G. Christophorou, J.K. Olthoff, Fundamental electron interactions with plasma processing gases, Kluwer Academic/Plenum, New York, 2004.
[113] V. Scheuer, H.W.P. Koops, T. Tschudi, Microelectron. Eng. 5 (1986) 423.
[114] D.A. Smith, J.D. Fowlkes, P.D. Rack, Nanotechnology 19 (2008) 415704.
[115] N. Silvis-Cividjian, C.W. Hagen, P. Kruit, J. Appl. Phys. 98 (2005) 084905/1.